

Sensorless Control of Induction Motors by the MSA based MUSIC Technique

Binying Ye*, STUDENT MEMBER IEEE

Maurizio Cirrincione*^{**}, SENIOR MEMBER IEEE

(*) Université Technologique de Belfort-Montbéliard
(UTBM)-OPERA, Belfort, France

binying.ye@utbm.fr

(**)University of the South Pacific (USP)

Suva,Fiji

m.cirrincione@ieee.org

Marcello Pucci#, SENIOR MEMBER IEEE,

Giansalvo Cirrincione##, SENIOR MEMBER IEEE

(#) Institute of Intelligent Systems for the Automation,
Palermo (ISSIA-CNR), Italy

marcello.pucci@ieee.org

(##) Université de Picardie Jules Verne

(UPJV), Amiens, France

g.cirrincione@ieee.org

Abstract—This paper proposes a speed sensorless technique for induction motor drives based on the retrieval and tracking of the rotor slot harmonics (RSH). The RSH related to the rotor speed is first extracted from the stator phase current signature by the adoption of two cascaded ADALINEs (ADaptive Linear Element), whose output is the estimated slot harmonic. Then, the frequency of this slot harmonic as well as the speed is estimated by using minor space analysis (MSA) EXIN neural networks, which work on-line to iteratively compute the frequency of the slot harmonics based on MUSIC spectrum estimation theory. Thanks to its sample-based learning and the reduced mean square frequency estimation error, the speed estimation is fast and accurate. The proposed sensorless technique has been experimentally tested on a suitably developed test set-up with a 2-kW induction motor drive. It has been verified that this algorithm can track the rotor speed rapidly and accurately in a very wide speed range, working from rated speed down to 1.3 % of it.

Keywords—induction motor; neural networks (NNs); minor space analysis (MCA); neural adaptive filtering; speed sensorless

I. INTRODUCTION

There has been extensive research in the sensorless field-oriented control (FOC) and direct-torque control (DTC) of induction motors (IMs) for the last two decades [1-25]. Both control methods require the accurate knowledge of the amplitude and angular position of the rotor or stator flux for ensuring the correct field orientation conditions. Additionally, information on the rotor angular velocity is required for velocity control over a wide speed range.

Among the main types of sensorless control, those tracking machine saliences [12-24] have a better performance at very low and zero speed: they are generally implemented by the injection of a high frequency voltage or current carrier, needed to excite the saliency itself [13]. A different approach lies in trying to track the rotor slotting effect directly, without any high frequency carrier excitation [15-24]. This leads up to an improved behavior of the drive in terms of reduced acoustic noise and torque ripple.

The spectral components of Rotor Slots Harmonics (RSHs) that can be observed in the stator current signature are given by [25],

$$f_h = (r q_r \mp n_d / n_p)(1-s)f_1 \mp v f_1 \quad (1)$$

where f_1 is the fundamental harmonic of the supply voltage, s the slip, p the number of pole pairs; n_d the eccentricity order, r the order of the space harmonic; v is the order of the time harmonics present in the power supply driving the motor, q_r the number of rotor slots per pole pair.

It should be noted, however, that the harmonics described in (1) are not present in a real machine for any combination of the number of rotor slots and pole pairs [25]; the upper sign refers to the case $q_r=3n-1$, and the lower one to the case $q_r=3n+1$, with $n \in \mathbb{N}$. In this analysis the stator slots for phase are supposed $3n$, so no stator slot harmonics are present.

The principal slot harmonic (PSH) refers to the first and prominent harmonic in the RSH series for an IM, obtained from eq. (1); indeed, with $v=1$, $r=1$, and if the higher-order time harmonics of the stator and rotor currents as well as the static and dynamical eccentricities are neglected ($n_d=0$), then the principal PSH is given by

$$f_h = q_r f_1 (1-s) \mp f_1 \quad (2)$$

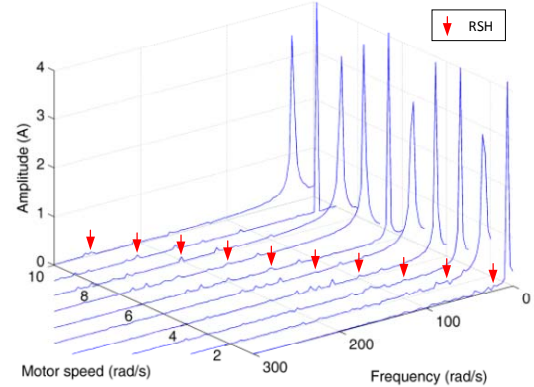


Fig. 1. FFT of the current signature of the IM at low speed from 1-10 rad/s, with 5Nm load (experiment)

Fig. 1 illustrates how the principal PSH changes with the motor speed in a 2kW motor (parameters and rated data are given in Tab. II), at 5Nm load condition. As compared to the fundamental frequency, it can be found from that the PSH appears at rather high ranges of the current spectrum at no-load; however, under load conditions, rotor slot harmonics tend to approach the harmonics of the machine and are harder to identify.

These harmonics can be directly exploited to successfully retrieve the instantaneous value of the rotor speed and position: it is obvious from (1) that the rotor speed (in hertz) can be computed by

$$f_r = (f_h \pm v f_1) / (r q_r \mp n_d / n_p) \quad (3)$$

This avoids increased acoustic noise, the reduction of the DC link voltage capability, the additional torque ripple and power losses caused by injected signals, and simplifies the signal processing system.

As for the direct rotor slot harmonic (PSH) tracking, two main approaches are followed in literature:

1) Frequency domain methods, mainly based on FFT (Fast Fourier Transform)-like approaches [15-18], such as the FFT, modern spectrum estimation methods, and chirp-Z transform.

2) Time domain methods, most of which are PLL (Phase-Locked Loop)-like approaches [19-21], such as the PLL and the adaptive digital filter.

Frequency domain methods generally provide good accuracy over a very wide speed range and load conditions, but a compromise has to be made between the required frequency resolution, to allow speed detection, and the response time versus changes of speed. A desired high frequency resolution demands the acquisition of a large amount of samples and a corresponding high acquisition time. Conversely, the time domain method provides a better real time performance than the frequency domain method, although the accuracy of the result will be affected by the noise level. The existing literature can generally work only in steady-state or in a specific speed range. Moreover, the capability of such methods to suitably track the rotor speed in transient conditions is not typically shown.

Alternatively, a great deal of existing subspace spectrum methods, such as the Pisarenko and MUSIC (MUltiple SIgnal Classification method) are based on the assumption that the signal is a sum of harmonics and explore the orthogonality between the noise subspace and the signal subspace [26-28]: they have the advantage of high estimation resolution and low variance, like most parametric spectrum methods, but are quite computationally time-consuming for real-time applications.

This paper aims to estimate the rotor speed on-line and proposes to solve the subspace method by using a recursive minor space analysis (MSA) neural network [29][30]. The overall system therefore combines the advantage of both the frequency domain methods (accuracy) and the time domain methods (speed of response). These advantages can be summarised as:

1) High pull-in capability so as to track the PSH in the entire speed range of the machine;

2) A flexible and selective bandwidth so as to simultaneously track the PSH in a wide range of variation without permitting any noise to enter the band of the detector;

3) Tracking properly the rotor speed even during speed transients (challenging task for an FFT-like method).

Once the signal is processed with a notch and a band filter, the output is a signal around a small frequency band. The on-line MUSIC algorithm permits to identify the PSH quickly and with accuracy, and is most useful for low speeds where the bandwidth of the band filter is larger and other harmonics are present.

The proposed sensorless technique has been implemented on a rotor flux oriented controlled drive and experimentally tested on a suitably developed test set-up with a 2-kW induction motor (IM) drive.

This paper is organized as follows. The cascaded ADALINE structure used to extract the rotor slot harmonic from the stator phase current is presented in section II. The MUSIC theory and the corresponding MSA EXIN neural solution are described in Section III and IV respectively. Finally, the comparative simulation and experiment results are provided in Section VI to assess the method.

II. ROTOR SLOT HARMONICS RETRIEVAL

A. Adaptive Linear Neural Filter

An adaptive linear neural filter based on a linear adaptive neuron (ADALINE) is a single layer artificial neural network which can be used as an adaptive notch filter or a band filter [31-33]. This means that the neuron is either able to cancel a determined signal at a certain frequency (notch filter), or it is able to let a determined signal pass at a predefined frequency (band filter, where band stands for a band of signals in a very narrow range around a predefined frequency).

The network presents two inputs and two outputs (fig.2): the primary input $d(k)$ is the signal to be processed; the reference input is a pure cosine wave and a pure cosine delayed of $\pi/2$, both of arbitrary amplitude C , with a pulsation ω_c equal to the pulsation of the harmonic of the primary input signal $d(k)$ that should be either eliminated (notch mode) or let pass (band mode); the two outputs give therefore the notch $\square(k)$ and the band $y(k)$ behaviour respectively.



Fig. 2. Schematic representation of the neural adaptive filter.

The procedure for updating the weights lies in a Least-Squares Algorithm (LS), such as the LMS or the TLS algorithm [30]. The LMS is adopted here because of its simplicity, low computational demand, and high-speed of convergence. A simple ADALINE with two neurons is adopted [33], and the on-line learning law is:

$$\begin{cases} w_1(k+1) = w_1(k) + 2\mu\varepsilon(k)x_1(k) \\ w_2(k+1) = w_2(k) + 2\mu\varepsilon(k)x_2(k) \end{cases} \quad (4)$$

where

$w_i(k)$ the weight of the i^{th} neuron at the k^{th} time sample;

μ the learning rate;

$\square(k)$ the difference between the primary input signal $d(k)$ and the band filter output $y(k)$; $\square(k)$ is also the notch filter output. k is the current discrete time sample.

It can be proved (see [32], p. 318, for the complete proof) that the notch transfer functions $H(z) = \varepsilon(z)/d(z)$ and band $K(z) = y(z)/d(z)$ are, respectively:

$$K(z) = \frac{2\mu C^2(z \cos(\omega_c) - 1)}{z^2 - 2(1 - \mu C^2)z \cos(\omega_c) + 1 - 2\mu C^2} \quad (5a)$$

$$H(z) = \frac{z^2 - 2z \cos(\omega_c) + 1}{z^2 - 2(1 - \mu C^2)z \cos(\omega_c) + 1 - 2\mu C^2} \quad (5b)$$

where $\varepsilon(z)$ and $d(z)$ are the z -transform of the sequences ε_k and d_k ; the transfer functions represent typical second order adaptive filters, like the SOGI-FLL in [34]. The dynamic and the filtering characteristics are completely defined by the learning rate μ and ω_c .

B. Scheme for the Retrieval of the PSH

To retrieve the harmonic component i_h caused by the PSH from the stator current signature, the structure shown in fig.3 is proposed: the PSH retrieval system is based on two cascaded ADALINEs: one (ADALINE 1) works in notch mode to eliminate the fundamental harmonic, the other (ADALINE 2) works in band mode to retrieve the PSH. This structure is particularly effective at very low speed range, as the PSH gets closer to the fundamental harmonic; indeed, a mere filtering approach in band mode in this condition would be more challenging, since it would require a much stronger attenuation of the ADALINE2 outside its passband to eliminate the fundamental, with resulting degradation of the dynamical performance.

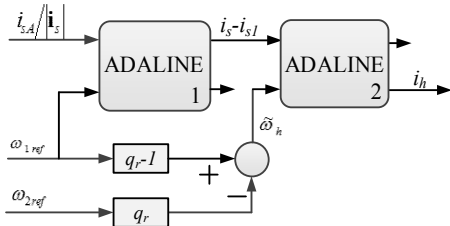


Fig. 3. ADALINE structure to track the PSH

ADALINE1 receives as an input the normalized stator phase current $i_{sA}(k)/|i_s|$ (so that a unit vector is used) given by

$$i_{sA}(k)/|i_s| = \left[\sum_{n=1, n \neq h}^{\infty} I_n \cos(\omega_n k + \varphi_n) \right] + I_h \cos(\omega_h k + \varphi_h) \quad (6)$$

while $\omega_{1\text{ref}}$ is the supply fundamental angular frequency. I_h , ω_h , φ_h are respectively the amplitude, angular frequency and initial phase of the PSH, and I_n , ω_n , φ_n are respectively, the amplitude, angular frequency and initial phase of the harmonics not including the PSH.

The ADALINE2 has as an input the output signal of the ADALINE1, as well as the estimated slot frequency \square_h . Since this paper takes into account only the principal PSH \square_h can therefore be directly computed by (2), using $\omega_{1\text{ref}}$ and the slip angular frequency $\omega_{2\text{ref}}$ as follows,

$$\tilde{\omega}_h = (q_r - 1)\omega_{1\text{ref}} - q_r \omega_{2\text{ref}} \quad (7)$$

$\omega_{1\text{ref}}$ is generally the supply fundamental frequency of the inverter, and its value in vector control schemes is estimated by the so called “current” model of the induction motor on the basis of the vector product between the rotor flux space vector and its derivative [1] while $\omega_{2\text{ref}}$ is obtained on the basis of the same “current model”.

$$\omega_{2\text{ref}} = \frac{L_m}{T_r |\Psi_r|^2} (\psi_{rd} i_{sQ} - \psi_{rq} i_{sD}) = \frac{2R_r}{3|\Psi_r|^2} t_e \quad (6)$$

where i_{sD} , i_{sQ} are the stator currents components in the stator reference frame, $|\Psi_r|$ is the amplitude of the rotor flux and ψ_{rd} , ψ_{rq} its components in the stator reference frame, t_e is the electromagnetic torque, L_m and T_r are respectively the three-phase magnetizing inductance and the rotor time constant.

It should be noted that, for obvious reasons, the estimated speed signal cannot be exploited to compute the value of $\omega_{1\text{ref}}$.

ADALINE 2 works in band mode and extracts the slot current i_h

$$i_h(k) = I_h \cos(\omega_h k + \varphi_h) \quad (7)$$

The noisy discrete-time measurements of this filtered slot harmonic can then be represented as

$$x(k) = i_h(k) + q(k) = I_h \cos(\omega_h k + \varphi_h) + q(k) \quad (8)$$

The noise $q(k)$ is assumed to be a zero-mean white process with unknown variance σ^2 .

The issue is now to find ω_h from K samples of $x(k)$. A great deal of existing subspace methods, such as Pisarenko and MUSIC, assume that the signal is a sum of harmonics and explore the orthogonality between the noise subspace and the signal subspace [26], and this results in having a good estimation resolution and performance. The MUSIC is an improvement of Pisarenko’s algorithm in terms of noise immunity and accuracy performance due to the ‘average effect’ of the noise subspace [26].

For p complex-valued harmonics, at least $p+1$ samples are needed ($p+1$ for Pisarenko’s method and more for MUSIC). But for p real-valued harmonics, at least $2p+1$ samples are needed due to the reason explained in section III.

III. THE MUSIC SPECTRUM ESTIMATION METHOD

The MUSIC algorithm assumes that the input signal $x(k)$ is a stationary random process made up of p complex exponentials and decomposes the autocorrelation matrix into two orthogonal matrices corresponding to signal- and noise-subspaces. Moreover assume the input $x(k)$ to be composed of M samples such that $\mathbf{x} = [x(1), x(2), \dots, x(M)]$, and affected by a white noise with variance σ^2 . Let \mathbf{R}_{xx} be the $M \times M$ autocorrelation matrix of vector \mathbf{x} , where $M > p+1$, it yields

$$\mathbf{R}_{xx} = E(\mathbf{x}\mathbf{x}^T) = \begin{bmatrix} r_{xx}(0) & r_{xx}(1) & \cdots & r_{xx}(M-1) \\ r_{xx}(1) & r_{xx}(0) & \cdots & r_{xx}(M-2) \\ \vdots & \vdots & \ddots & \vdots \\ r_{xx}(M-1) & r_{xx}(M-2) & \cdots & r_{xx}(0) \end{bmatrix} \quad (9)$$

Where $r_{xx}(k)$ is the autocorrelation sequence such that

$$r_{xx}(k) = E\{x(n+k)x^*(n)\} = E\{x^*(n)x(n+k)\} = r_{xx}^*(-k) \quad (10)$$

Where $E\{\cdot\}$ is the expectation function of the random process (ensemble average)..

If the eigenvalues of \mathbf{R}_{xx} are arranged in increasing order, $\lambda_M \leq \lambda_{M-1} \leq \dots \leq \lambda_1$, and the corresponding orthonormal eigenvectors are $\mathbf{z}_M, \mathbf{z}_{M-1}, \dots, \mathbf{z}_1$, then, these eigenvectors may be divided into two groups, the p ‘signal eigenvector’ corresponding to the p largest eigenvalues and the ($q=M-p$) ‘noise eigenvectors’ with the associated eigenvalues equal to σ^2 . Since \mathbf{R}_{xx} is Hermitian, the eigenvectors $\mathbf{z}_i (i=1, \dots, M)$ form an orthonormal set. Therefore, the signal and noise subspaces are orthogonal, i.e., for any vector \mathbf{u} in the signal subspace and for any vector \mathbf{v} in the noise subspace, $\mathbf{u}^H \mathbf{v} = 0$ (see [26] for complete proof).

Each of the $M-p$ eigenvectors $\mathbf{v}_i = [v_i(0), v_i(1), \dots, v_i(M-1)]^T$ is orthogonal to each of the signal vectors, $\mathbf{e}_i = [1 \ e^{j\omega} \ e^{j2\omega} \ \dots \ e^{j(M-1)\omega}]^T (i=1, \dots, p)$. This means that

$$V_i(e^{j\omega}) = \sum_{k=0}^{M-1} v_i(k) z^{-jk\omega} = \mathbf{e}^H \mathbf{v}_i \quad i=p+1, \dots, M, \quad (13a)$$

where $\mathbf{e} = [1 \ e^{j\omega} \ e^{j2\omega} \ \dots \ e^{j(M-1)\omega}]^T$. Remark that (13a) is null for each of the ω_i (the p pulsations composing the input signal). Therefore, the z-transform of each noise eigenvector, that is the eigenfilter $V_i(z)$, is given by

$$V_i(z) = \sum_{k=0}^{M-1} \mathbf{v}_i(k) z^{-k} \quad i=p+1, \dots, M, \quad (11b)$$

Each i -th eigenfilter will have obviously $M-1$ roots, of which ideally p lie on the unit circle ($|z|=1$) for (13a). In this way from any one of the eigenfilters the p pulsations of the input signal $x(k)$ can be retrieved by taking the angles of these roots. Moreover the eigenspectrum

$$P_{MUSIC}(e^{j\omega}) = \frac{1}{\left| \sum_{k=0}^{M-1} v_i(k) e^{-jk\omega} \right|^2} \quad (14a)$$

will have sharp peaks in correspondence of the p pulsations of the input signals. However, the remaining $M-p-1$ roots can lie anywhere in the complex plane, possibly even close to the unit circle giving rise to other spurious peaks to this eigenspectrum. On the other hand there are $M-p$ redundant ‘eigenfilters’, so that $M-p$ sets of results can be get from MUSIC algorithm, allowing spurious peaks to be reduced by using an average of all of these results, by using the following eigenspectrum:

$$P_{MUSIC}(e^{j\omega}) = \frac{1}{\sum_{i=p+1}^M |\mathbf{e}^H \mathbf{v}_i|^2} \quad (12b)$$

Conversely, the well-known Pisarenko’s algorithm can be regarded as a particular case of the MUSIC with $p=1$, meaning no redundancy is used to attenuate spurious peaks

It must be noted that this application require only the estimation of the frequency components of the signal and not of their amplitude, but MUSIC and Pisarenko methods can also estimate the amplitude if needed.

It is obvious that p real-valued harmonics (ex. the PSH) are equal to $2p$ complex exponentials, since the real-valued input $\cos(\omega t)$ is convenient to be represented as $(e^{j\omega t} + e^{-j\omega t})/2$.

However, it is quite cumbersome to carry out the MUSIC algorithm since it is based on the eigen-decomposition which is computationally cumbersome when the dimension M becomes big (with $O(M^3)$ computational complexity).. In the following, a neural solution will be presented, which improves the computational burden.

IV. THE MSA MUSIC METHOD

An iterative solution for MUSIC method can be obtained by using the minor space analysis (MSA) neural networks, which are generally an extension of minor component analysis (MCA) neural networks [29][30].

Let a linear neuron be considered with a real input vector $\mathbf{x}(k) = [x_1(k), \dots, x_M(k)]^T$ and with output $y(k)$:

$$y(k) = \mathbf{w}^T(k) \mathbf{x}(k) = \sum_{i=1}^M w_i(k) x_i(k) \quad (13)$$

where $\mathbf{w}(k) = [w_1(k), \dots, w_M(k)]^T$ is the weight vector. In this case, $\mathbf{x}(k)$ is the time samples of the filtered slot harmonic given by (10) (with noise), e.g. the output of ADALINE2, and the number of the weights of the MSA neural network is chosen in accordance with the dimension of the autocorrelation matrix as detailed before. In convergence the weights represent the components of the eigenvectors corresponding to the minimum eigenvalues of the autocorrelation matrix of the input data. The output is the residual and in convergence goes to zero.

The MCA EXIN, one of the best MCA neuron in terms of stability and converging time, whose average gradient flow (ODE) is directly derived from the gradient flow of RQ,

$E[J] = \frac{\mathbf{w}^T \mathbf{R}_{xx} \mathbf{w}}{\mathbf{w}^T \mathbf{w}}$ [29], has the following learning law,

$$\mathbf{w}(k+1) = \mathbf{w}(k) - \frac{\alpha(k)y(k)}{\|\mathbf{w}(k)\|^2} \left[\mathbf{x}(k) - \frac{y(k)\mathbf{w}(k)}{\mathbf{w}^T(k)\mathbf{w}(k)} \right] \quad (14)$$

Where $\alpha(k)$ is the learning rate.

By using the adaptive Gram-Schmidt ortho-normalization and (16), the MSA EXIN learning law is given in [30] as,

$$\begin{aligned} \mathbf{w}_j(t+1) &= \mathbf{w}_j(t) - \frac{\alpha(t)y_j(t)}{\|\mathbf{w}_j(t)\|^2} \times \\ &\left[\mathbf{x}(t) - \sum_{i>j} y_i(t)\mathbf{w}_i(t) - \frac{\mathbf{w}_j^T(t)(\mathbf{x}(t) - \sum_{i>j} y_i(t)\mathbf{w}_i(t))\mathbf{w}_j(t)}{\mathbf{w}_j^T(t)\mathbf{w}_j(t)} \right] \end{aligned} \quad (15)$$

Where $j=M, M-1, \dots, M-q+1$. Let \mathbf{R}_{xx} be the $M \times M$ autocorrelation matrix, then if $\mathbf{w}_j(0)$ satisfies $\mathbf{w}_j^T(0)\mathbf{z}_j \neq 0$ (being \mathbf{z}_j the orthonormal eigenvector in the noise subspace), it holds that the weight vectors converge to the minor subspace spanned by the corresponding minor components, thus it is orthogonal to all the signal vectors, and can be used to replace \mathbf{v}_i in (14) where the frequencies are computed.

For the data coming from ADALINE2, given by eq. (10), the following values are chosen: $M=5$, and $p=2$, so that the dimension of the subspace is $q=3$. It is considered that as output of the ADALINE2 has only one harmonic PSH presents, and the noise subspace dimension is chosen to be 3 due to a trade-off between computational complexity and estimation accuracy. Fig.4 shows the corresponding MSA neurons structure for noise subspace retrieval with $p=2, q=3$.

Remark that $p=2$ is the number of complex frequencies, so as explained at the end of section III, only one harmonic is estimated.

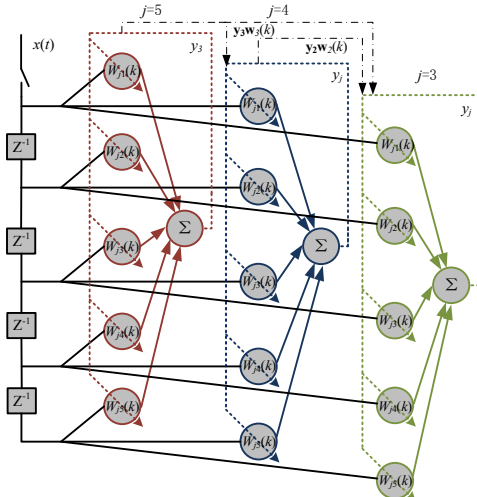


Fig. 4. MSA EXIN neural network structure for noise eigenvec estimation

The effect of increment in noise subspace has been shown in fig.5, where the MSA MUSIC (with 3 noise eigenvectors) has been compared with the MCA Pisarenko's algorithm (with 1 noise eigenvector; computed by the MCA neural network). The input is a sinusoid contaminated by white noise (SNR=20dB), whose frequency varies between 0.15π and 0.125π . It is obvious from fig.5b that the frequency estimation

error of MSA MUSIC is smaller than the MCA Pisarenko's algorithm.

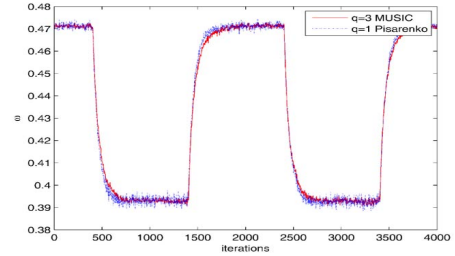


Fig. 5. frequency estimation results of the MSA MUSIC compared with the MCA Pisarenko's algorithm

TABLE I. COMPARISON OF THE STEADY-STATE PERFORMANCE

SNR	10 dB		20dB		30dB		
	Methods	MCA	MSA	MCA	MSA	MCA	MSA
Mean value		0.1266π	0.1257π	0.1252π	0.1251π	0.1250π	0.1250π
Variance		2.31e-5	6.74e-6	1.76e-6	4.89e-7	1.68e-7	2.44e-8

The statistical performance of the two algorithms (MCA Pisarenko's method and MSA MUSIC method) at different noise level is shown in Tab.1. The signal pulsation is 0.125π . It can be found that the accuracy of MSA MUSIC increases significantly with increase of noise subspace and fewer peaks are present due to the averaging effect.

V. TEST SET-UP

The employed test set-up consists of:

- A three-phase induction machine with parameters shown in Tab.1, with 36 stator and 28 rotor slots.
- An 8 kVA, three-phase VSI for the control of the machine side inverter.
- A torque controlled brushless Interior Mounted Permanent Magnet (IMPM) machine drive for the load.
- A dSPACE card (DS1103) with a PowerPC 604e at 400 MHz and a floating-point DSP TMS320F240 for the control of the machine side inverter.

TABLE II. PARAMETERS OF THE INDUCTION MACHINE

Rated power Prated [kW]	2.2
Rated voltage Urated [V]	220
Rated frequency frated [Hz]	50
Pole-pairs	2
Stator resistance Rs [Ω]	2.9
Stator inductance Ls [mH]	223
Rotor resistance Rr [Ω]	1.52
Rotor inductance Lr [mH]	229
3-phase magnetizing inductance Lm [mH]	217
Moment of inertia J [$\text{kg}\cdot\text{m}^2$]	0.0048

The space-vector dynamic model of the IM including rotor slotting effects, which was proposed in [25] is used for the simulation part. Table II shows the parameters of the IM used in the experimental rig and in the simulations.

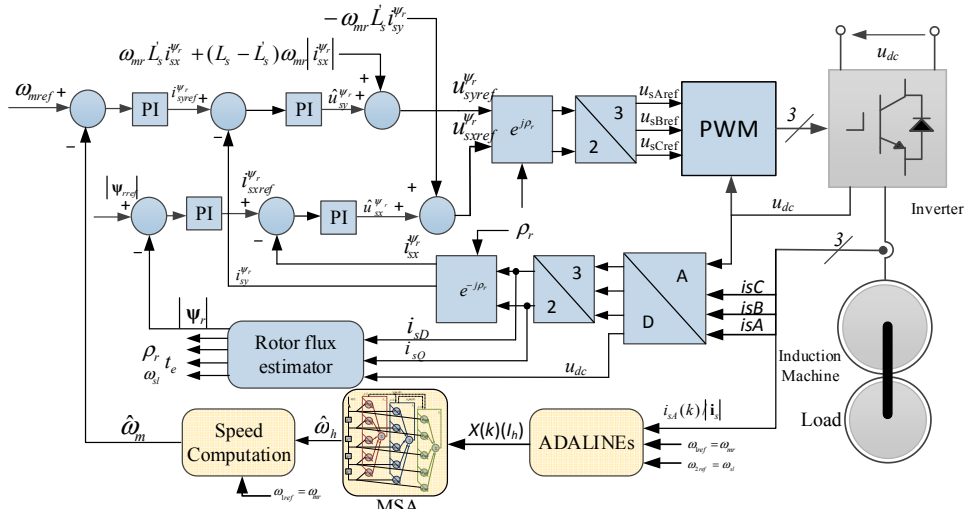


Fig. 6. Implement field oriented scheme and speed estimation scheme

VI. RESULTS

The speed estimation performance is assessed in the framework of the measured speed based vector control system: a VSI direct rotor-flux oriented vector control [field oriented control (FOC)] (as shown in fig. 6) in which current control is performed at the field reference frame level. The proposed on-line speed estimator is connected along with the main vector control loop, and the variables $\omega_{1\text{ref}}$ and $\omega_{2\text{ref}}$, which are used for the reference of the two ADALINEs, are respectively taken from the “current” flux model based on the rotor equations of the machine written in the rotor flux oriented reference frame. The output of the estimator is fed back to close the speed control loop.

In the following some selected simulation and experimental results of the proposed speed estimator are shown, trying to emphasise the correct behaviour of the estimator in a wide speed range.

The tracking capability results are shown in figs. 7 – 10, when a speed step is given as reference, from 10 rad/s to 5 rad/s, with a 5Nm load. Fig. 7 and fig. 8 show the simulation results, while fig.9 and fig.10 show the corresponding experimental results under the same condition. Fig.7 shows that in simulation the estimated speed tracks the measured speed properly: even during the transient, the estimated speed converges to the true one, and the speed of response is quick. Particularly, it should be noted that the MUSIC algorithm is able to track very fast (step) speed variations in the low speed working region in presence of a load torque, which is a in general a challenging task for any sensorless technique, while it is something very new for any FFT-based technique. It should be noted that 5 rad/s corresponds to 3.3% of the rated speed, as expected.

Fig. 8 shows the current at the input and output of the ADALINE2. The slot current is well extracted from the stator current.

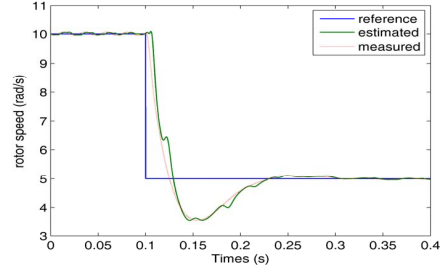


Fig. 7. simulation result of speed tracking when speed steps down from 10 rad/s to 5 rad/s with 5Nm load

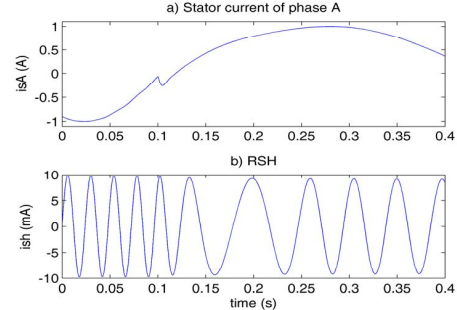


Fig. 8. normalized stator phase i_{sa} and the output of ADALINE2 i_h

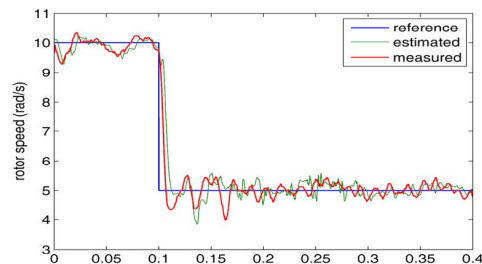


Fig. 9. experimental result of speed tracking when speed steps down from 10 rad/s to 5 rad/s with 5 Nm

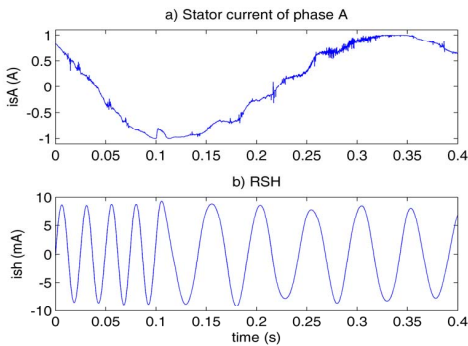


Fig. 10. experiment normalized stator phase i_{sa} and the output of ADALINE2 i_h when speed step down from 10 to 5 rad/s

Fig. 9 and fig.10 show that in the experiment, the overall behaviour of the system ties up with the one in the simulation. Although the phase current signature in the experiment presents a number of harmonics, the output of ADALINE2 is apparently correct in estimating the PHS, and the speed tracking performance is very satisfactory.

The rejection capability to load torque steps at low speed is shown in figs.11-14: the motor operates at constant speed of 10 rad/s (6.6% of the rated speed), the load torque step occurs at $t=1$ s, from 0Nm to 5Nm. Fig.11 and 12 show the simulation results, while fig.13 and 14 show the corresponding experiment results.

From fig. 11, it can be found that the drive is robust to load torque step variations, and the estimated speed tracks the measured and reference speeds properly in about 0.5s, with a very good dynamic performance.

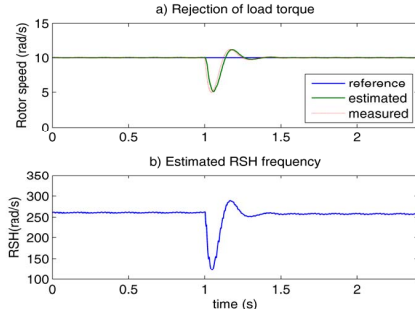


Fig. 11. simulation result of load torque steps when motor operates at 10 rad/s

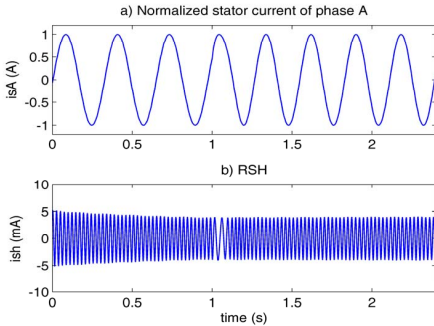


Fig. 12. simulation result of normalized stator phase i_{sa} and the output of ADALINE2 i_h

As shown in fig. 13 and 14, experimental results are obtained in accordance to the simulation ones.

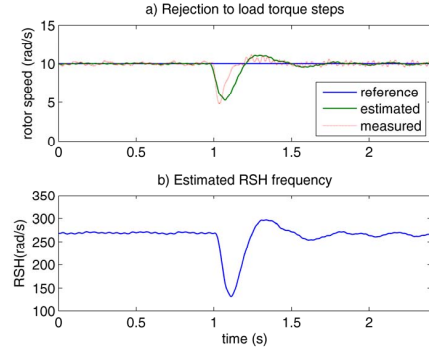


Fig. 13. result of load torque steps when motor operates at 10 rad/s

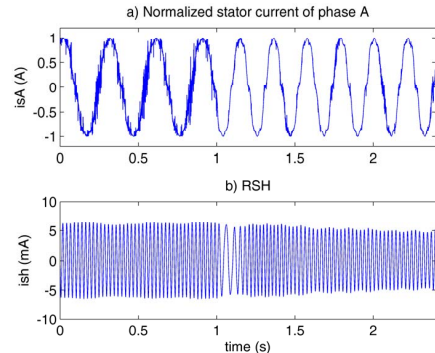


Fig. 14. experimental result of normalized stator phase i_{sa} and the output of ADALINE2 i_h

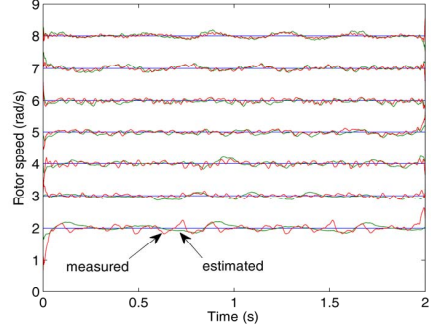


Fig. 15. steady-state performance of the proposed method

VII. CONCLUSIONS

This paper proposes a speed sensorless technique for induction motor drives based on the retrieval and tracking of the rotor slot harmonic. The speed related rotor slot harmonic is extracted from the stator phase current by two ADALINES: one works in notch mode in order to eliminate the fundamental current, the other works in band mode thus its output consists only of the slot harmonic. The frequency of this extracted slot harmonic is then estimated by using the MSA EXIN neural networks as a fundamental tool for applying on-line the MUSIC algorithm, which exploits the orthogonality between the noise subspace and the signal subspace for estimating frequencies present in a signal. With

an augmented noise subspace dimension, the estimated results with MUSIC can be ‘averaged’, leading up to a very small frequency estimation error with less noisy estimated signal. Thus, the overall speed estimation algorithm is quick and accurate. Furthermore, the performance of the overall system has been verified both in simulation and experimentally, on a suitably developed test set-up. The experimental results are in good accordance with the simulation ones, confirming the validity of the proposed method and showing that it is quite competitive even at low speed ranges, down to 1.3 % of the rated speed.

REFERENCES

- [1] P. Vas, “Sensorless Vector and Direct Torque Control”, Oxford Science Publication, 1998.
- [2] Cirrincione M, Pucci M, Vitale G. Power Converters and AC Electrical Drives with Linear Neural Networks[M]. CRC Press, 2012.
- [3] Holtz J. Sensorless control of induction motor drives[J]. Proceedings of the IEEE, 2002, 90(8): 1359-1394.
- [4] Ghane M, Zheng G. On sensorless induction motor drives: Sliding-mode observer and output feedback controller[J]. Industrial Electronics, IEEE Transactions on, 2009, 56(9): 3404-3413.
- [5] Kim S H, Park T S, Yoo J Y, et al. Speed-sensorless vector control of an induction motor using neural network speed estimation[J]. Industrial Electronics, IEEE Transactions on, 2001, 48(3): 609-614.
- [6] Hu, J.; Wu, B., "New integration algorithms for estimating motor flux over a wide speed range," Power Electronics Specialists Conference, 1997. PESC '97 Record., 28th Annual IEEE , vol.2, no., pp.1075,1081 vol.2, 22-27 Jun 1997
- [7] Hurst, K.D.; Habetler, T.G.; Griva, G.; Profumo, F., "Zero-speed tacholess IM torque control: simply a matter of stator voltage integration," Industry Applications, IEEE Transac-tions on , vol.34, no.4, pp.790,795, Jul/Aug 1998
- [8] Holtz, J.; Juntao Quan, "Sensorless vector control of induction motors at very low speed using a nonlinear inverter model and parameter identification," Industry Applications, IEEE Transactions on , vol.38, no.4, pp.1087,1095, Jul/Aug 2002
- [9] Orlowska-Kowalska, T.; Dybkowski, M., "Stator-Current-Based MRAS Estimator for a Wide Range Speed-Sensorless Induction-Motor Drive," Industrial Electronics, IEEE Transactions on , vol.57, no.4, pp.1296,1308, April 2010
- [10] Cirrincione, M.; Accetta, A.; Pucci, M.; Vitale, G., "MRAS Speed Observer for High-Performance Linear Induction Motor Drives Based on Linear Neural Networks," Power Electronics, IEEE Transactions on , vol.28, no.1, pp.123,134, Jan. 2013
- [11] Kyo-Beum Lee; Blaabjerg, F., "Reduced-order extended luenberger observer based sensor-less vector control driven by matrix converter with nonlinearity compensation,"Industrial Electronics, IEEE Transactions on , vol.53, no.1, pp.66,75, Feb. 2006
- [12] J. Holtz, “Sensorless control of induction machines—With or without signal injection?,” IEEE Trans. Ind. Electron., vol. 53, no. 1, pp. 7–30, Feb. 2006.
- [13] Caruana, C.; Asher, G.M.; Sumner, M., "Performance of HF signal injection techniques for zero-low-frequency vector control of induction Machines under sensorless conditions," Industrial Electronics, IEEE Transactions on , vol.53, no.1, pp.225,238, Feb. 2006
- [14] F. Briz, M. W. Degner, A. Diez, R. D. Lorenz, “Static and Dynamic Behavior of Saturation-Induced Salienties and their Effect on Carrier – Signal – Based Sensorless AC Drives”, IEEE Transactions on Industry Applications, vol. 38, n. 3, pp. 670-678, May/June 2002
- [15] Blasco-Gimenez, R.; Asher, G.M.; Sumner, M.; Bradley, K.J., "Performance of FFT-rotor slot harmonic speed detector for sensorless induction motor drives," Electric Power Applications, IEE Proceedings - , vol.143, no.3, pp.258,268, May 1996
- [16] Ferrah, A.; Bradley, K.J.; Asher, G.M., "An FFT-based novel approach to noninvasive speed measurement in induction motor drives," Instrumentation and Measurement, IEEE Transactions on , vol.41, no.6, pp.797,802, Dec 1992
- [17] Hurst, K.D.; Habetler, T.G., "A comparison of spectrum estimation techniques for sensorless speed detection in induction machines," Industry Applications Conference, 1995. Thirtieth IAS Annual Meeting, IAS '95., Conference Record of the 1995 IEEE , vol.1, no., pp.553,559 vol.1, 8-12 Oct 1995
- [18] Aiello, M.; Cataliotti, A.; Nuccio, S., "An induction motor speed measurement method based on current harmonic analysis with the chirp-Z transform," Instrumentation and Measurement, IEEE Transactions on , vol.54, no.5, pp.1811,1819, Oct. 2005
- [19] Ferrah, A.; Bradley, K.J.; Hogben-Laing, P.J.; Woolfson, Malcolm S.; Asher, G.M.; Sumner, M.; Cilia, J.; Shuli, J., "A speed identifier for induction motor drives using real-time adaptive digital filtering," Industry Applications, IEEE Transactions on , vol.34, no.1, pp.156,162, Jan/Feb 1998
- [20] Yamamoto, K.; Iimori, K.; Morita, H., "A study of digital filter for rotor speed detection with slot harmonic current for induction motor," TENCON 2010 - 2010 IEEE Region 10 Conference , vol. , no., pp.2137,2142, 21-24 Nov. 2010
- [21] Zhi Gao; Turner, L.; Colby, R.S.; Leprette, B., "A Frequency Demodulation Approach to Induction Motor Speed Detection," Industry Applications, IEEE Transactions on , vol.47, no.4, pp.1632,1642, July-Aug. 2011
- [22] Pucci, M.; Serporta, C., "Finite-Element Analysis of Rotor Slotting Saliency in Induction Motors for Sensorless Control," Magnetics, IEEE Transactions on , vol.46, no.2, pp.650,653, Feb. 2010
- [23] Staines, C.S.; Caruana, C.; Asher, G.M.; Sumner, M., "Sensorless control of induction Machines at zero and low frequency using zero sequence currents," Industrial Electronics, IEEE Transactions on , vol.53, no.1, pp.195,206, Feb. 2006
- [24] Raute, R.; Caruana, C.; Staines, C.S.; Cilia, J.; Sumner, M.; Asher, G.M., "Sensorless Control of Induction Machines at Low and Zero Speed by Using PWM Harmonics for Rotor-Bar Slotting Detection," Industry Applications, IEEE Transactions on , vol.46, no.5, pp.1989,1998, Sept.-Oct. 2010
- [25] M. Cirrincione , M. Pucci , G. Cirrincione , A. Miraoui, “Space-Vector State Model of Induction Machines Including Rotor Slotting Effects: Towards a New Category of Observers”, IEEE Transactions on Industry Applications, Vol. 44, n.6, November/December 2008.
- [26] Hayes M H. Statistical digital signal processing and modelling [M]. John Wiley & Sons, 2009.
- [27] Kay, Steven M., and Stanley Lawrence Marple Jr. "Spectrum analysis—a modern perspective." Proceedings of the IEEE 69.11 (1981): 1380-1419.
- [28] Stoica, Petre; Nehorai Arye, "MUSIC, maximum likelihood, and Cramer-Rao bound," Acoustics, Speech and Signal Processing, IEEE Transactions on , vol.37, no.5, pp.720,741, May 1989.
- [29] Cirrincione, G.; Cirrincione, M.; Herault, J.; Van Huffel, S., "The MCA EXIN neuron for the minor component analysis," Neural Networks, IEEE Transactions on , vol.13, no.1, pp.160,187, Jan 2002
- [30] Cirrincione G, Cirrincione M. Neural-Based Orthogonal Data Fitting: The EXIN Neural Networks[M]. John Wiley & Sons, 2011.
- [31] Cirrincione M, Pucci M, Vitale G. A single-phase DG generation unit with shunt active power filter capability by adaptive neural filtering[J]. Industrial Electronics, IEEE Transactions on, 2008, 55(5): 2093-2110.
- [32] B. Widrow, S. D. Stearns, Adaptive Signal Processing, Signal Processing Series, Prentice-Hall, Englewood Cliffs, NJ, 1985.
- [33] Cirrincione, M., Pucci, M., Vitale, G., & Miraoui, A. (2009). Current harmonic compensation by a single-phase shunt active power filter controlled by adaptive neural filtering. Industrial Electronics, IEEE Transactions on, 56(8), 3128-3143.
- [34] Rodriguez, P.; Luna, A.; Muñoz-Aguilar, R.S.; Etxeberria-Otadui, I.; Teodorescu, R.; Blaabjerg, F., "A Stationary Reference Frame Grid Synchronization System for Three-Phase Grid-Connected Power Converters Under Adverse Grid Conditions," Power Electronics, IEEE Transactions on , vol.27, no.1, pp.99,112, Jan. 2012